Earthquakes and Structures, *Vol. 12, No. 3 (2017) 297-307*
DOI: https://doi.org/10.12989/eas.2017.12.3.297

Development of seismic collapse capacity spectra for structures with deteriorating properties

Zhan Shu[1], Shuang Li*[2,3], Mengmeng Gao[2,3] and Zhenwei Yuan[2,3]

[1]*Department of Structural Engineering, Tongji University, Shanghai, 200092, China*
[2]*Key Lab of Structures Dynamic Behavior and Control of the Ministry of Education, Harbin Institute of Technology, Harbin 150090, China*
[3]*Key Lab of Smart Prevention and Mitigation of Civil Engineering Disasters of the Ministry and Information Technology, Harbin Institute of Technology, Harbin 150090, China*

(Received August 7, 2016, Revised January 16, 2017, Accepted February 8, 2017)

Abstract. Evaluation on the sidesway seismic collapse capacity of the widely used low- and medium-height structures is meaningful. These structures with such type of collapse are recognized that behave as inelastic deteriorating single-degree-of-freedom (SDOF) systems. To incorporate the deteriorating effects, the hysteretic loop of the nonlinear SDOF structural model is represented by a tri-linear force-displacement relationship. The concept of collapse capacity spectra are adopted, where the incremental dynamic analysis is performed to check the collapse point and a normalized ground motion intensity measure corresponding to the collapse point is used to define the collapse capacity. With a large amount of earthquake ground motions, a systematic parameter study, i.e., the influences of various ground motion parameters (site condition, magnitude, distance to rupture, and near-fault effect) as well as various structural parameters (damping, ductility, degrading stiffness, pinching behavior, accumulated damage, unloading stiffness, and P-delta effect) on the structural collapse capacity has been performed. The analytical formulas for the collapse capacity spectra considering above influences have been presented so as to quickly predict the structural collapse capacities.

Keywords: seismic collapse; collapse capacity; ground motion parameters; deteriorating hysteretic behaviors; analytical predictions

1. Introduction

Severe earthquakes may cause structural collapses, which lead to huge replacement financial costs as well as the death and downtime costs. Collapse prevention, which requires deep understanding of structural collapse capacities, has been the primary performance target for the seismic design. Despite the challenging nature of seismic collapse assessment, increased research efforts over these years try to lead to a better understanding of structural collapse.

To estimate the structural peak responses under earthquakes in a simple way, the response spectra method has been widely used in design practices. The studies on inelastic response spectra are booming over these years under the framework of performance-based earthquake engineering (Riddell *et al.* 2002, Chopra and Chintanapakdee 2004, Thermou *et al.* 2012, Dimakopoulou *et al.* 2013, Han *et al.* 2014, Katsanos and Sextos 2015, Esfahanian and Aghakouchak 2015, Rahgozar *et al.* 2016). The existing inelastic response spectra generally belong to constant-strength spectra or constant-ductility spectra, whose specific yielding strength levels or ductility levels of the SDOF system are predefined, respectively. The constant-strength spectra present the seismic responses for SDOF systems with known yielding strength but it is not relevant to sthe structural collapse state. Although the ductility could be used to label the collapse state, it is also well recognized that the values of Damage Measure (DM) of a structure corresponding to collapse state are different from one ground motion record to another, rather than a predefined ductility value. Therefore, the constant-ductility spectra can represent some damage states of the structure, but it is not capable to fully represent the real responses at the collapse state.

With the advent of analysis technology, structural collapse could be evaluated by the Incremental Dynamic Analysis (IDA) approach (Vamvatsikos and Cornell 2002). After the definition of structural collapse capacity and criterion to judge the collapse state, the IDA can be used to check the collapse state and then calculate the collapse capacity and corresponding response spectra. Ibarra and Krawinkler (2011) assumed the collapse of SDOF system occurs when the loading path is on the backbone curve and the restoring force approaches zero, and performed parametric studies on the collapse capacity spectra of the structures subjected to earthquake excitations. Ibarra and Krawinkler's study was later followed and extended by Shi *et al.* (2014) to study the influences of hysteretic model parameters on the collapse capacity spectra. In studies (Adam and Jäger 2011, Adam and Jäger 2012, Jäger and Adam 2013), the collapse capacity of inelastic non-deteriorating SDOF structures vulnerable to the P-delta

*Corresponding author, Associate Professor
E-mail: shuangli@hit.edu.cn

http://www.techno-press.com/journals/eas&subpage=7
ISSN: 2092-7614 (Print), 2092-7622 (Online)

effect and near-fault effect was studied, where the collapse of SDOF system is at the loss of its stability (IDA curve becomes horizontal) or over a predefined ductility limit. Although studies have been done on the effects of some ground motion features and structural properties on structural collapse capacity spectra, further studies are needed to give a more comprehensive understanding of these spectra (i.e., systematic parameter influences come from ground motions and structures themselves) and to facilitate their practical applicability (i.e., suitable collapse state criterion for design, and easily used formula representations).

The presented study tries to extend the existing work related with evaluation on seismic structural collapse. The study considers the structural deteriorating effects in addition to the P-delta effect. The systematic parametric studies on structural collapse capacity have been performed, include the influences from ground motion parameters such as the site condition, earthquake magnitude, distance to rupture, and near-fault effect and the influences from various structural parameters based on a larger amount of earthquake ground motion records. In addition, to facilitate the implementation of the collapse capacity evaluation, the study fits the calculated collapse capacity spectra curves into the analytical formulas, which allows a quick prediction of the hazard of collapse in structures during severe earthquake events.

2. Seismic collapse capacity spectra

Fig. 1(a) illustrates a SDOF system with inelastic spring characteristics utilizing the mechanical model. The rigid rod of length l is assumed massless and simply supported. The inelastic properties of the structural model are assigned to a rotational elastic-plastic spring at the base. The variable K_e denotes the initial rotational stiffness of the spring. A rotational viscous dashpot damper with damping parameter c_r is connected in parallel to the spring. At the tip of the rod the system is subjected to the gravity load P. For a base acceleration $\ddot{x}_g$, which excites the structure to vibrations, the nonlinear equation of motion can be derived in terms of the rotation angle $\theta(t)$ as shown in Eq. (1). The equation is assumed that the angle of rotation is small (i.e., when $|\theta(t)| \ll 1$, $\sin\theta(t)=\theta(t)$, $\cos\theta(t)=1$)

$$ml^2\ddot{\theta}(t) + c_r\dot{\theta}(t) + M[\theta(t)] - Pl\theta(t) = -ml\ddot{x}_g \tag{1}$$

A stability coefficient χ is defined equal to Pl/K_e, which characterizes the static stability of the corresponding elastic system subjected to the gravity load. If $\chi<1$ the equilibrium of the statically loaded elastic structure is stable, otherwise it is unstable. The definition of the ductility μ is equal to $\theta(t)/\theta_y$, and $\overline{f}_s$, the normalized moment, is defined as $M[\theta(t)]/M_y$, where $M_y = f_y\, l$ is the yielding moment and f_y is the yielding base shear force.

Then Eq. (1) could be reformed in term of μ as

$$\frac{1}{\omega^2}\ddot{\mu} + 2\xi\frac{1}{\omega}\dot{\mu} + (\overline{f}_s - \chi\mu) = -\frac{\ddot{x}_g}{g\gamma} \tag{2}$$

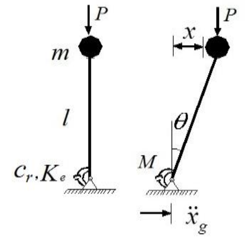

(a) Mechanical model of SDOF

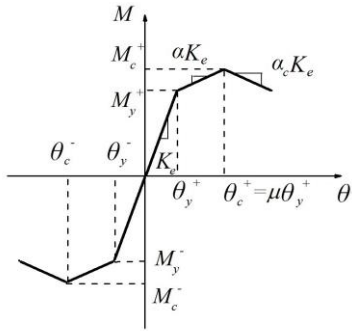

(b) Hysterical backbone curve

Fig. 1 SDOF model and the tri-linear hysterical backbone curve

where the natural circular frequency ω, the viscous damping ratio ξ, and the yield strength coefficient γ are given by

$$\omega = \sqrt{\frac{K_e}{l^2 m}},\quad \xi = \frac{c_r}{2\omega l^2 m},\quad \gamma = \frac{M_y}{lmg} = \frac{f_y}{mg} \tag{3}$$

The tri-linear backbone curve illustrated in Fig. 1(b) is adopted to represent the nonlinear deteriorating behavior of the SDOF system. The hysteretic loop matches the "Hysteretic material" model in the OpenSees software platform (2015). Such nonlinear behavior could be fully defined by six parameters: (1) The initial stiffness K_e; (2) The yielding strength M_y; (3) The post-yielding stiffness αK_e; (4) The yield deformation θ_y and deformation θ_c at maximum strength defined by the nominal ductility ratio μ_n (μ_n is defined as θ_c/θ_y); (5) The degrading stiffness $\alpha_c K_e$; (6) The unloading stiffness (defined by $\mu_n^{-\beta}K_e$, where β is the power used to determine the degraded degree of the unloading stiffness based on ductility). In addition, the hysteretic model can also consider the pinching behavior and accumulated damage effects. In the following study on the influences of earthquake ground motions, a "standard" hysteretic model with constant parameters and 5% damping ratio is defined (see Section 5); meanwhile, the parameters in the "standard" hysteretic model change when study on the influences of the structural properties is performed.

In this study, the definition of structural collapse capacity is inherited from the previous work (Ibarra and Krawinkler 2011, Adam and Jäger 2011, Adam and Jäger 2012, Jäger and Adam 2013, Shi *et al.* 2014), which uses a dimensionless Intensity Measure (IM), i.e., scaled spectral acceleration $S_{a,i}(T)$ at the structural initial period T corresponding to structural collapse occurrence normalized by the gravity acceleration g and the base shear coefficient

$\gamma=f_y/mg$. For the i^{th} ground motion record, the collapse capacity spectral value CC_i is defined as

$$IM\,|_{S_{a,i}(T)} = CC_i = \left.\frac{S_{a,i}(T)}{g\gamma}\right|_{\text{collapse}} \quad (4)$$

At the state of collapse an infinitesimal increase of the ground motion intensity leads to large unbounded deformation. Since “unbounded” is not an easy numerical implementation, this study uses the collapse state according to the FEMA 20% tangent slope approach (FEMA350, 2000), which defines the point on the IDA curve with a tangent slope reduces to 20% of the initial elastic slope to be the capacity point. Generally speaking, such a criterion of collapse state is more suitable to practical engineering applications because in design or evaluation procedures for real buildings, the collapse limit is seldom set as the point when the loading path is on the backbone curve and the restoring force approaches zero to guarantee enough redundancy; meanwhile, the judgment of a 20% tangent slope is easier than that judgment of an unstable state in numerical calculations.

The use of seismic collapse capacity spectra defined by Eq. (4) for structural collapse capacity evaluation or design is straightforward. In an evaluation procedure, the $\gamma=f_y/mg$ is known because the structural property is known, therefore $S_{a,i}(T)$ corresponding to collapse state can be determined; Otherwise in a design procedure, $S_{a,i}(T)$ corresponding to collapse state is known because it can be seemed as same with the maximum design load, therefore $\gamma=f_y$/mg can be determined, i.e., the minimum structural design yielding base shear f_y to avoid collapse can be determined. Because the spectra are derived by SDOF models, it can be used directly for the SDOF structures; for the multiple-degree-of-freedom (MDOF) structures, such as the low- and medium-height structures considered in this study, their equivalent SDOF systems can be used.

3. Selected ground motion assembly

A sufficient number of earthquake ground motion records need to be selected to obtain better collapse capacity spectra. By doing so the record-to-record ground motion uncertainties could be statistically relieved, which makes a study more meaningful. This study selected 382 far-fault ground motion records from the Pacific Earthquake Engineering Research Center (PEER). A total count of 86, 100, 100, and 96 records are for the four site conditions, i.e., the site class B, C, D, and E based on the catalog of USGS, respectively. Table 1 provides a summary of the selected far-fault ground motions, where the moment magnitude of the earthquake ground motion records ranges from 6.52 to 7.62 and their PGA ranges from 0.05 g to 1.07 g.

Near-fault ground motions often show impulsive characteristics exhibiting distinguishable pulses in their velocity time histories, significantly imposing higher demands on structures (Malhotra 1999, Alavi and Krawinkler 2004, Li and Xie 2007). Therefore, besides the far-fault ground motion records, this study adopted another 91 near-fault ground motion records identified by Baker (2007) using the wavelet analysis to represent earthquakes showing the near-fault effect.

Table 1 Selected far-fault ground motions

Earthquake event	Time of the event	Magnitude	Number
Chi-Chi, Taiwan	1999/09/20	7.62	58
Northridge, America	1994/01/07	6.69	52
Kobe, Japan	1995/01/16	6.90	12
Tottori, Japan	2000/10/06	6.61	48
Niigata, Japan	2004/10/23	6.63	30
Chuetsu-oki, Japan	2007/07/16	6.80	34
Iwate, Japan	2008/06/13	6.90	44
El Mayor-Cucapah, Mexico	2010/04/04	7.20	8
Loma Prieta, Japan	1989/10/18	6.93	30
San Fernando, America	1971/02/09	6.61	16
Duzce, Turkey	1999/11/12	7.14	2
San Simeon, CA, America	2003/12/22	6.52	2
Imperial Valley-06, America	1979/10/15	6.53	16
Hector Mine, America	1999/10/16	7.13	18
Irpinia, Italy-01	1980/11/23	6.90	4
Landers, America	1992/06/28	7.28	4
Kocaeli, Turkey	1999/08/17	7.51	2
Superstition Hills-02, America	1987/11/24	6.54	2

4. Influences of the earthquake ground motions

The far-fault ground motion records are categorized by different site conditions, magnitudes, and distances to rupture. The collapse capacity spectra of the far-fault ground motions are also compared with those of the near-fault ground motions to show the influence from the impulsive features in earthquakes on the collapse capacity. The coefficient of variation (CV) spectra are given to test the dispersion of the collapse capacity spectra.

4.1 Influence of site condition

The collapse capacity spectra and their CVs for site conditions B, C, D, and E are presented in Fig. 2. The general trend of the collapse capacity spectra is close for all the four site conditions. For short period structures, the collapse capacity spectral values linearly increase to approximate 3.0 with the increase of structural period. The collapse capacity spectral values reaches its plateau when

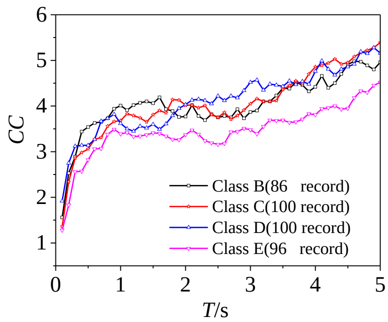

(a) Collapse capacity spectra

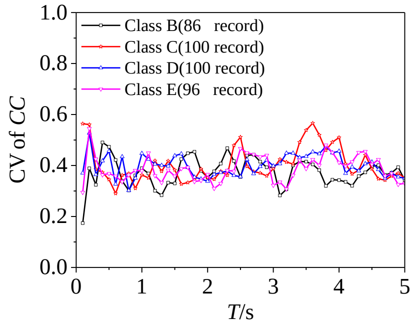

(b) CVs

Fig. 2 Collapse capacity spectra for different site conditions and their CVs

about 0.3 s<T≤3.0 s. For long period structures, the collapse capacity spectral values slightly increase to near 5.0. Out of the four selected site conditions, the collapse capacity spectral values for site E is obviously smaller than those of other site conditions. The collapse capacity spectral values for site E are about 20% smaller than those from the other sites. Therefore, the soft soil condition for site E is proved detrimental for structural collapse capacities. The collapse capacity spectra for different site conditions yield acceptable dispersions, which are shown from their CV spectra with values fluctuate near 0.4.

4.2 Influence of earthquake magnitude

In order to explore the effects due to the influence of earthquake moment magnitude M, the selected far-fault ground motions are sorted into three subsets (i.e., 114 records with M≤6.65, 146 records with 6.65<M≤6.9, and 122 records with M>6.9). The collapse capacity spectra for the three subsets of earthquake magnitude are presented in Fig. 3(a). It could be noticed that the collapse capacity spectral values are relatively smaller for larger earthquake magnitudes when structural periods are small (i.e., T≤0.9 s). When the structural periods is larger than 1.0, the collapse capacity response curves cross with each other for different levels of earthquake magnitude, showing a weak correlation between the earthquake magnitude and the structural collapse capacity. Generally speaking, the influence of earthquake magnitude is marginal. Fig. 3(b) shows the CVs for the collapse capacity spectra, which fluctuate within acceptable range.

4.3 Influence of distance to rupture

In addition to the site condition and the earthquake magnitude, the site distance to the source might also influence the collapse capacity of a structure. In order to explore the collapse capacity spectra trend under the

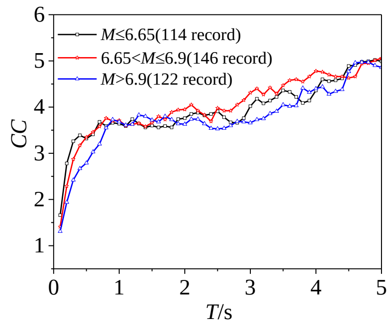

(a) Collapse capacity spectra

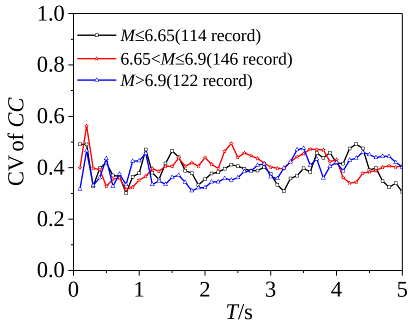

(b) CVs

Fig. 3 Collapse capacity spectra for different earthquake magnitudes and their CVs

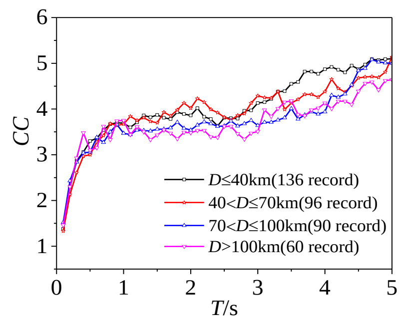

(a) Collapse capacity spectra

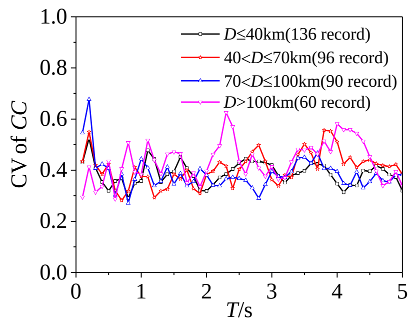

(b) CVs

Fig. 4 Collapse capacity spectra for different distance to rupture and their CVs influence of the distance to rupture, the selected far-fault ground motions are sorted into four subsets with different ranges of distance (i.e., the so-called shortest distance from a site to a rupture surface, 136 records with distance smaller than 40 km, 96 records with 40 km$<D\leq$70 km, 90 records with 70 km$<D\leq$100 km, and 60 records with distance larger than 100 km). The collapse capacity spectra and their CVs for the four subsets of records are presented in Fig. 4. It could be concluded from Fig. 4(a) that the influence from distance on the collapse capacity spectra is not significant. Fig. 4(b) shows the CVs for the corresponding collapse capacity spectra which are also acceptable.

4.4 Influence of near-fault effect

The near-fault ground motions usually demonstrate impulsive characteristics, which are commonly believed to cause severe structural damages. The collapse capacity spectra and their CVs are presented in Fig. 5 to compare the collapse capacity spectra derived from the far-fault and near-fault ground motions. It could be concluded from Fig. 5 that the near-fault effect reduces the structural collapse capacity spectral values around to 15% for structural periods smaller than about 2.4s. This result agrees with the observations in previous studies (Jäger and Adam 2013, Shi *et al.* 2014), in which the near-fault effect reduces the collapse capacity of short- and medium-period structures. However, for structures with larger periods, the observation shows that reduction of collapse capacity spectral values due to near-fault effect is not significant. The CV spectra presented in Fig. 5(b) has shown that the collapse capacity spectra for the near-fault ground motions also yields acceptable dispersion.

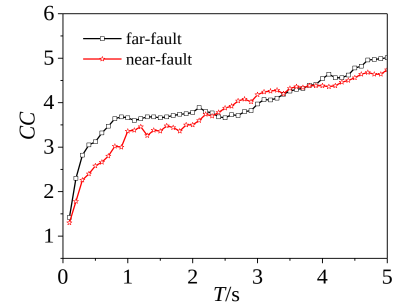

(a) Collapse capacity spectra

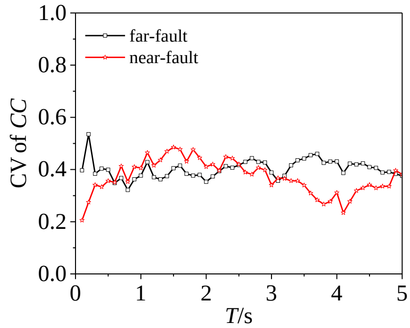

(b) CVs

Fig. 5 Collapse capacity spectra for far-fault and near-fault ground motions and their CVs

5. Influences of the structural properties

This section explores the collapse capacity spectra due to the influence of various structural properties including the system damping, the material level nonlinearities, and the geometric level nonlinearities. The "standard" hysteretic behavior of the model defined as the SDOF system with parameters μ_n=3.0, α=0, α_c=0.5, *pinchX*=1.0, *pinchY*=1.0, *damage1*=0, *damage2*=0, χ-α=0, and β=0 by the "Hysteretic material" model (Opensees 2015) is shown in Fig. 6(a), whose envelope curve is tri-linear referring to Fig. 1(b). For a generalized civil structure, considering that the post-yielding stiffness ratio α is usually within 5% of the structural elastic stiffness, α is set zero for the study. Fig. 6 also presents a set of force-displacement illustrations to show different post-yielding behaviors compared with the standard model. Fig. 6(b) shows the influence of nominal ductility ratio μ_n on the loop. Fig. 6(c) shows the change of backbone curve strength reduction due to a modification of degrading stiffness. The hysteretic model allows the pinching effect for both strength (defined by *pinchY*) and displacement (defined by *pinchX*), which constrains the development of force or displacement as shown in Fig. 6(d). Fig. 6(e) and Fig. 6(f) define the hysteretic relation considering two types of structural damage (i.e., structural damages due to ductility and structural damages due to the reduction of energy dissipation capacity). Then, the unloading stiffness degradation effect is illustrated in Fig. 6(g). Finally, Fig. 6(h) superposes the negative slope imposed by the P-delta effect.

5.1 Influence of viscous damping ratio

Four levels of damping ratios are selected for

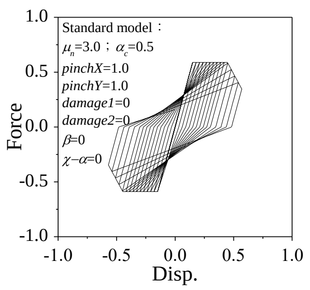

(a) The hysteretic loop - Standard model

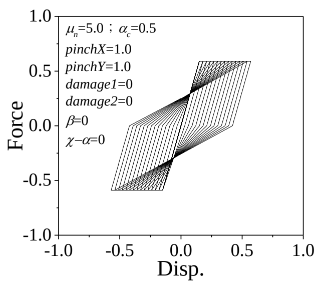

(b) Behavior with a larger nominal ductility ratio

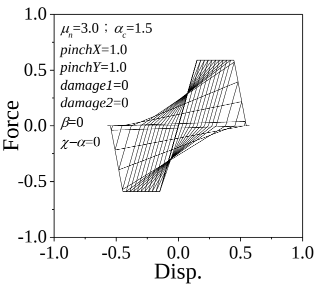

(c) Behavior with a larger degrading stiffness

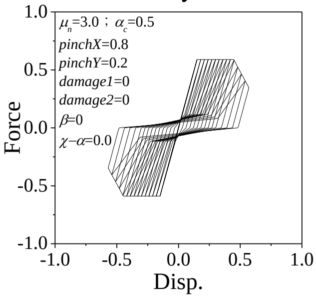

(d) Incorporating the pinching effect

Fig. 6 Normalized hysteretic properties with different model parameters

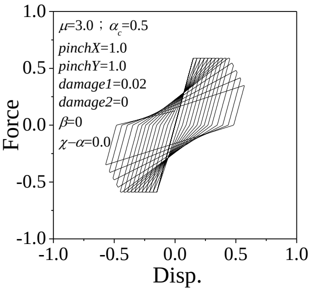

(e) Incorporating ductility-dependent damage

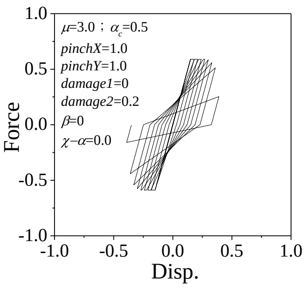

(f) Incorporating energy-dependent damage

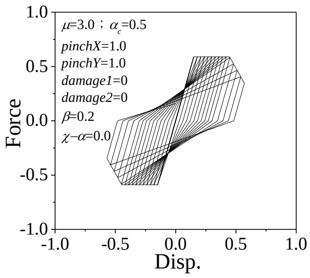

(g) Incorporating the unloading stiffness

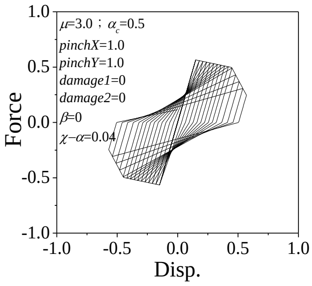

(h) Incorporating the P-delta effect

Fig. 6 Continued

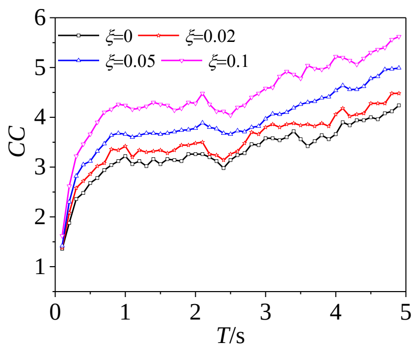

(a) Collapse capacity spectra

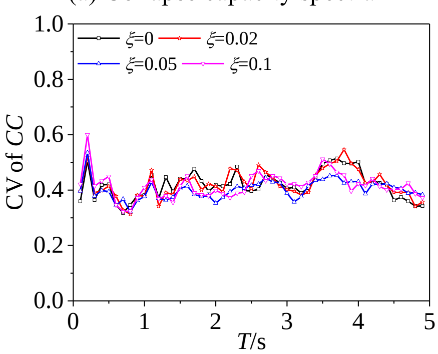

(b) CVs

Fig. 7 Collapse capacity spectra for different damping ratios and their CVs

calculation of collapse capacity, i.e., ξ=0, 2%, 5%, and 10%. The collapse capacity spectra for the four damping ratios are presented in Fig. 7(a). It could be noticed from Fig. 7(a) that the damping ratio is a considerable influence factor on structural collapse capacities. Differences among the collapse capacity spectra curves for the different damping ratio are significant. A larger damping ratio (e.g., 10%) could help increase structural collapse capacity by 30%-60% compared with the un-damped case. For intermediate level of damping ratio (e.g., 5%), the structural collapse capacity could increase at least 15% at the most periods. This matches the fact that structures that have smaller system damping are usually more vulnerable to collapse compared with structures with larger structural damping ratios.

5.2 Influence of nominal ductility ratio

The collapse capacity spectra for μ_n=2.0, 3.0, 4.0, 5.0, and 6.0 are presented in Fig. 8(a). One could conclude that a structure with larger ductility could have higher collapse capacity against earthquakes. The collapse capacity spectra curves have proved the benefit of larger nominal ductility ratios, commonly regarded as "better" structural designs against collapse. Specifically, increasing the nominal ductility ratio from 2.0 to 6.0 could double the collapse capacity over the structural periods between 0s<T≤5s. The increase of seismic collapse capacity by providing more nominal ductility ratio is decreasing. For example, to secure a 4.0 collapse capacity for structures with periods larger than 1.0s, μ_n should be 4.0 or more. However, to secure a 5.0 collapse capacity, μ_n should be designed to be greater than 6.0. The CV spectra corresponding to the five collapse capacity spectra curves are presented in Fig. 8(b). The dispersions grow larger when the nominal ductility is larger. Nonetheless, all the dispersions stay within the acceptable range.

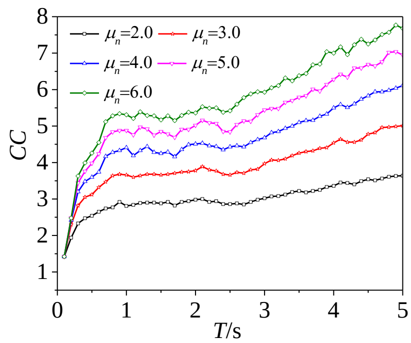

(a) Collapse capacity spectra

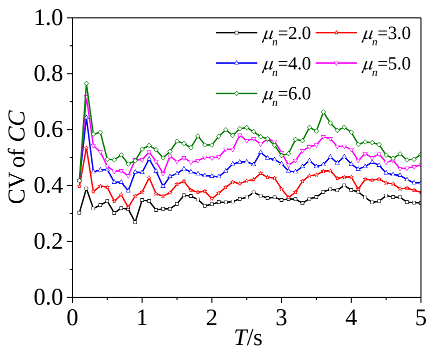

(b) CVs

Fig. 8 Collapse capacity spectra for different nominal ductility ratios and their CVs

5.3 Influence of degrading stiffness

According to the tri-linear backbone curve illustrated in Fig. 1(b), after the maximum strength of a structure is reached (strength corresponding to normal ductility ratio), the strength starts to degrade. The degrading stiffness ratio α_c is defined as the absolute value of degrading stiffness of the third segment of the backbone curve divided by the elastic stiffness. The study selects four degrading stiffness ratios that are 0.5, 1.0, 1.5, and 2.5. The collapse capacity spectra and their CVs are presented in Fig. 9. According to Fig. 9(a), the general trends of collapse capacity spectra are similar regardless of the degrading stiffness ratios. It could be noticed that when α_c is larger than 1.0, the difference among the three collapse capacity spectra are small. Whereas the difference of the collapse capacity between α_c=0.5 and α_c=1.0 is relatively large. When structural period is about 5.0, the collapse capacity for α_c=0.5 is about 20% higher than the case when α_c=1.0. In addition, the collapse capacity spectra for the four different degrading stiffness ratios yield acceptable dispersion.

5.4 Influence of pinching behavior

In the hysteretic model, *pinchX* defines the pinching effect on the displacement and *pinchY* defines the pinching effect on the strength. When *pinchX*=*pinchY*=1.0, there are no pinching effects. This study selects the value of *pinchX* and *pinchY* from 0.2 to 1.0 in order to see their influences on structural collapse capacities. From Fig. 10(a), it could be found that the displacement pinching effects are only marginal in terms of structural collapse capacities. The corresponding CVs are presented in Fig. 10(b), which are reasonably small. However, the strength pinching effect is significant. When small strength pinching happens, collapse capacity spectra significantly decrease due to the changed unloading mechanism and less energy dissipation capacities associated with the pinching model. The collapse capacity spectra considering the strength pinching effect and their CVs are presented in Fig. 10(c) and Fig. 10(d), respectively. When *pinchY*=0.2, the largest strength pinching effect happens, reducing the collapse capacity by 45% near T=1.8 s. The decrease of the collapse capacities mainly happen over the structural periods between 0 s and 4.0 s. For a flexible structure when T=5.0 s, the adverse effects by strength pinching becomes ignorable. Dispersions of the collapse capacity spectra with strength pinching effect are presented in Fig. 10(d).

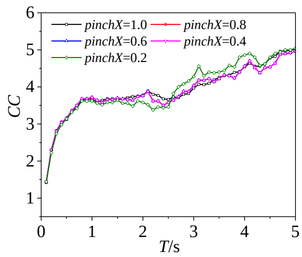

(a) Displacement pinching collapse capacity spectra

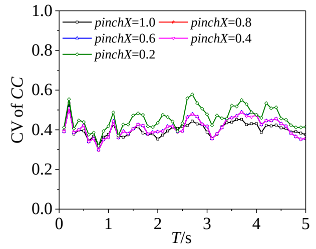

(b) CVs

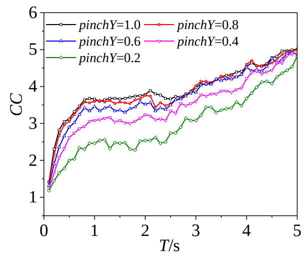

(c) Force pinching collapse capacity spectra

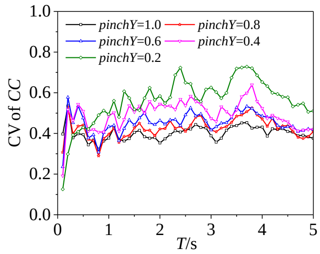

(d) CVs

Fig. 10 Collapse capacity spectra for different pinching effects and their CVs

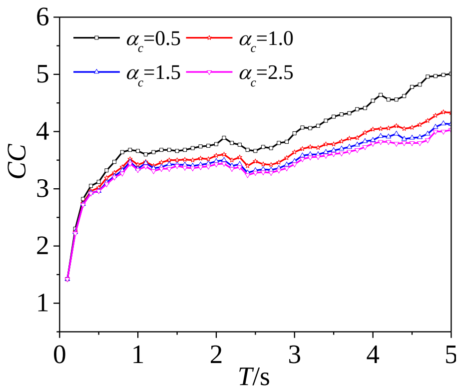

(a) Collapse capacity spectra

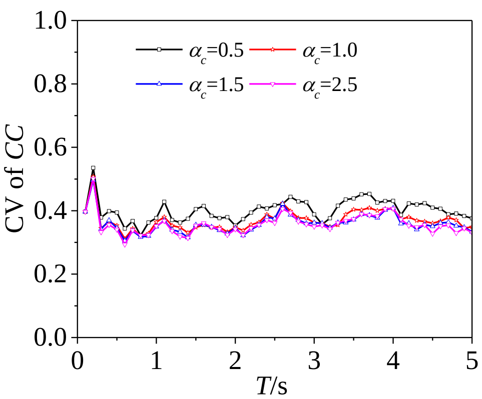

(b) CVs

Fig. 9 Collapse capacity spectra for different degrading stiffness ratios and their CVs

5.5 Influence of accumulated damage

The variable *damage1* captures the structural ductility-dependent damages. This means that the strength reduction caused by *damage1* index is proportional to the displacement level, *i.e.*, the larger the displacement the larger the strength reduction. When *damage1* become larger, the damage becomes more severe. Five numerical values, from 0 (not considering the damage) to 0.08, are selected for the variable *damage1*. The collapse capacity spectra for the five levels of such damage are presented in Fig. 11(a). It could be seen from the figures that after considering damages, structural collapse capacities decreases. Compared with the case considering no damage (i.e., *damage1*=0), the *damage1*=0.08 case reduce the collapse capacities for about 15% at the most periods. From Fig. 11(b), the corresponding CVs for collapse capacity spectra of the first type of damage are within the acceptable range.

The variable *damage2* captures the structural energy-dependent damages. This means that the strength reduction caused by *damage2* index is proportional to the energy dissipated by the history of inelastic displacement, i.e., the strength reduction increases with the number of cycles even if at a fixed displacement level. When *damage2* become larger, the damage becomes more severe. This study selects six different values for the variable *damage2* starting from 0 (not considering the damage) to 0.4. The collapse capacity spectra for the six levels of damage are presented in Fig. 11(c). It could be concluded from the figure that *damage2* is more violent than *damage1* in terms of the reduction of the structural collapse capacity. Compared with the case considering no damage (i.e., *damage2*=0), the *damage2*=0.05 case reduce the collapse capacities for about 30%-50% at the most periods. For the case when *damage2*=0.4, the structural collapse capacity spectrum curve is almost a linear curve whose collapse capacities was abruptly reduced to less than 2.0. From Fig. 11(d), the corresponding CVs for collapse capacity spectra of the second type of damage are small and acceptable.

5.6 Influence of unloading stiffness

The mathematical expression of the unloading stiffness is $\mu_n^{-\beta}K_e$, which is a function of the nominal ductility ratio μ_n, the degraded unloading stiffness factor β, and the elastic stiffness K_e. The larger β is, the more unloading stiffness degrades, reducing the area within the hysteretic loop. The collapse capacity spectra for β=0, 0.2, 0.4, and 0.6 are presented in Fig. 12(a). It could be seen that the collapse capacity spectra curves are similar when β=0, 0.2, 0.4, and 0.6. Therefore, the study concludes that the influence from the unloading stiffness is not significant for consideration in the structural collapse capacity spectra. The corresponding dispersions for the collapse capacity spectra are small according to Fig. 12(b).

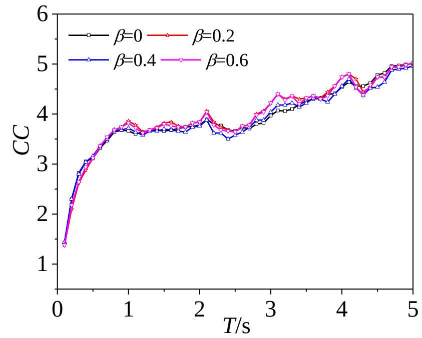

(a) Collapse capacity spectra

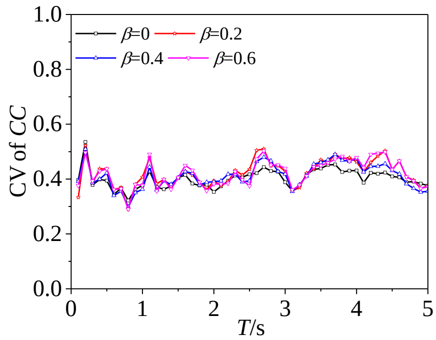

(b) CVs

Fig. 12 Collapse capacity spectra for different unloading stiffness and their CVs

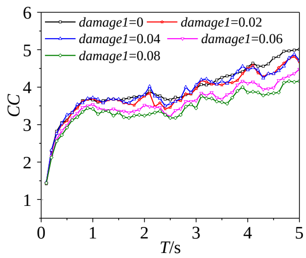

(a) Collapse capacity spectra considering ductility-dependent damage

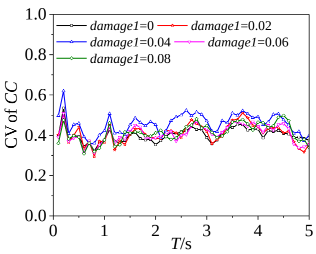

(b) CVs

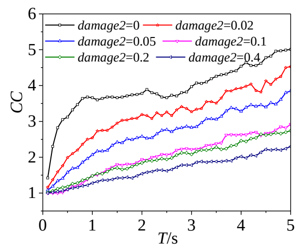

(c) Collapse capacity spectra considering energy-dependent damage

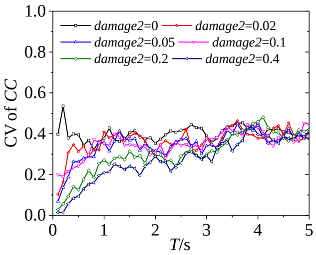

(d) CVs

Fig. 11 Collapse capacity spectra for different damage levels and their CVs

5.7 Influence of P-delta effect

The P-delta effect is presented in terms of the elastic stability coefficient χ, which depends on the characteristics of the structure being represented with an equivalent SDOF system (see Section 2). The stiffness of the equivalent SDOF system is modified based on the hysterical backbone curve shown in Fig. 1(b), where the K_e becomes $(1-\chi)K_e$, αK_e becomes $(\alpha-\chi)K_e$, and $\alpha_c K_e$ becomes $(\alpha_c-\chi)K_e$. As the default post-yielding stiffness ratio for this study is 0, the numerical value of χ could fully define the P-delta effect. This study selects five elastic stability coefficients, i.e., χ-α=0, 0.04, 0.08, 0.12, and 0.16. The collapse capacity spectra for the five levels of P-delta effect are presented in Fig. 13(a). As a result, the five collapse capacity spectra share similar trends over the structural period 0 s<T≤5.0 s. Also evidenced by the figure is that the collapse capacity decreases about 30%-40% as χ increases from 0 to 0.16 at the most periods. The result proves again that the P-delta effects are detrimental for the collapse resistant capacity of a generalized nonlinear structure (Jäger and Adam 2013,

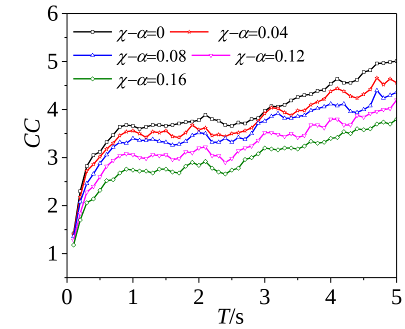

(a) Collapse capacity spectra

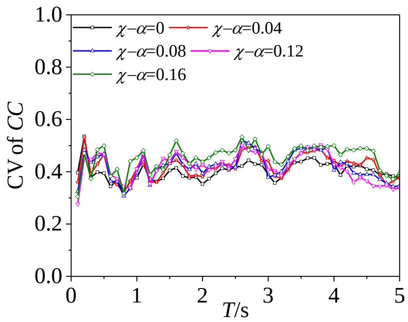

(b) CVs

Fig. 13 Collapse capacity spectra for different levels of P-delta effect and their CVs

Shi *et al.* 2014). The corresponding CVs for the collapse capacity spectra are presented in Fig. 13(b), indicating that the dispersions are acceptable for all the levels of P-delta effect.

6. Fitting analytical formulas

The above sections have parametrically analyzed the influences of ground motion properties and structural properties on the structural collapse capacities. To facilitate the implementation of the presented work in practical applications, this section fitted the corresponding analytical formulas for prediction of structural collapse capacity. The numerical fitting procedure adopts the improved algorithm with quasi-Newton method. The fitting of the collapse capacity spectra for all far-fault ground motions and the base case using the standard hysteretic model is first presented as

$$CC_{base} = \frac{0.958 + 90.879T^2}{1 + 25.231T^2 - 0.3T^4} \tag{5}$$

In addition to the collapse capacity spectrum for the base case, another nine adjustment coefficients (the effects of earthquake magnitude, distance to rupture, and unloading stiffness can be neglected) are established to consider all the various influences mentioned above. The comprehensive collapse capacity spectra could be defined as

$$CC = c_1 c_2 CC_{base} \tag{6}$$

where c_1 and c_2 are the influence coefficients of ground motion properties and structural properties, respectively, which are defined as

$$c_1 = \phi_1\phi_2 \tag{7a}$$

$$c_2 = \varphi_1\varphi_2\varphi_3\varphi_4\varphi_5\varphi_6\varphi_7 \tag{7b}$$

where the detailed mathematical expressions of the nine coefficients are presented by Eq. (8). The two coefficients ϕ_1 and ϕ_2 account for the soft soil effect from site condition E and the near-fault effect, are functions of structural period T. The damping adjustment coefficient φ_1 is a function of structural period T and viscous damping ratio ξ; the ductility adjustment coefficient φ_2 is a function of structural period T and normal ductility ratio μ_n; the degrading stiffness adjustment coefficient φ_3 is a function of structural period T and the degrading stiffness ratio α_c; the pinching adjustment coefficient φ_4 is a function of structural period T and the strength pinching variable pY (i.e., *pinchY*); the damage adjustment coefficients φ_5 and φ_6 are functions of structural period T and the damage variables dmg_1 and dmg_2 (i.e., *damage1* and *damage2*); the P-delta effect adjustment coefficient φ_7 is a function of structural period T, the stability coefficient χ, and the post-yielding stiffness ratio α. Fig. 14 presents the analytical collapse capacity spectra fitted by the above formulas together with the statistical data. The solid lines represent the fitted curves and the dotted lines represent the ones from the statistical analyses. The 'all site conditions' result in Fig. 14(a) are determined as average values between those obtained for site condition B, C, D, and E. It could be concluded that the fitting is reasonably close to the statistical data

$$\phi_1(T) = 0.904 - 0.003T^2 + 0.002\exp(T) \tag{8a}$$

$$\phi_2(T) = 0.872T^{0.124T - 0.024T^2} \tag{8b}$$

$$\varphi_1(T,\xi) = 0.887 - 0.092T + 0.07T^2 - 0.019T^3 + 0.002T^4 + 2.859\xi \tag{8c}$$

$$\varphi_2(T,\mu_n) = \begin{cases} \dfrac{0.65 - 0.643T + 0.108\mu_n}{1 - 1.04T + 0.3T^2 + 0.03\mu_n} & T \le 1.0\text{s} \\ -0.586 + 1.001T^{0.024}\mu_n^{\,0.396} & T > 1.0\text{s} \end{cases} \tag{8d}$$

$$\varphi_3(T,\alpha_c) = 0.952 - 0.118T^{0.024} + 0.07T^2 - 0.019T^3 + 0.02T^4 + 0.067/\alpha_c \tag{8e}$$

$$\varphi_4(T,pY) = \frac{-0.478 + 0.134T + 0.074T^2 + 14.977pY}{1 + 0.346T + 13.537pY} \tag{8f}$$

$$\begin{aligned}\varphi_5(T,dmg_1) &= 0.751 - 0.06T + 0.024T^2 \\ &- 0.003T^3 + 0.0018dmg_1^{\,-1} - 0.0002dmg_1^{\,-2}\end{aligned} \tag{8g}$$

$$\varphi_6(T,dmg_2) = -0.255 + 0.459T^{0.155} + 0.122dmg_2^{\,-0.383} \tag{8h}$$

$$\begin{aligned}\varphi_7(T,\chi-\alpha) &= 0.982 - 0.677(\chi-\alpha) \\ &- 4.687(\chi-\alpha)^2 + 0.145\exp(-T/0.079)\end{aligned} \tag{8i}$$

7. Conclusions

The seismic collapse capacity spectrum is a useful tool to evaluate the sidesway collapse resistant capacity of the low- and medium-height structures. In the study, when calculating the collapse capacity spectra, the deteriorating effects are incorporated to represent a more realistic structural behavior. Under a large number of ground motion records, the judgment of the collapse state by FEMA 20% tangent slop approach, and a comprehensive study of influence factors, the developed collapse capacity spectra are recognized as an extension to the existing studies since it is more reliable and suitable to be used in practical engineering applications. The comprehensive study of influence factors on the collapse capacity spectra includes various ground motion parameters (site condition, magnitude, distance to rupture, and near-fault effect) as well as structural parameters (damping, ductility, degrading stiffness, pinching behavior, accumulated damage, unloading stiffness, and P-delta effect). The study leads to the following conclusions:

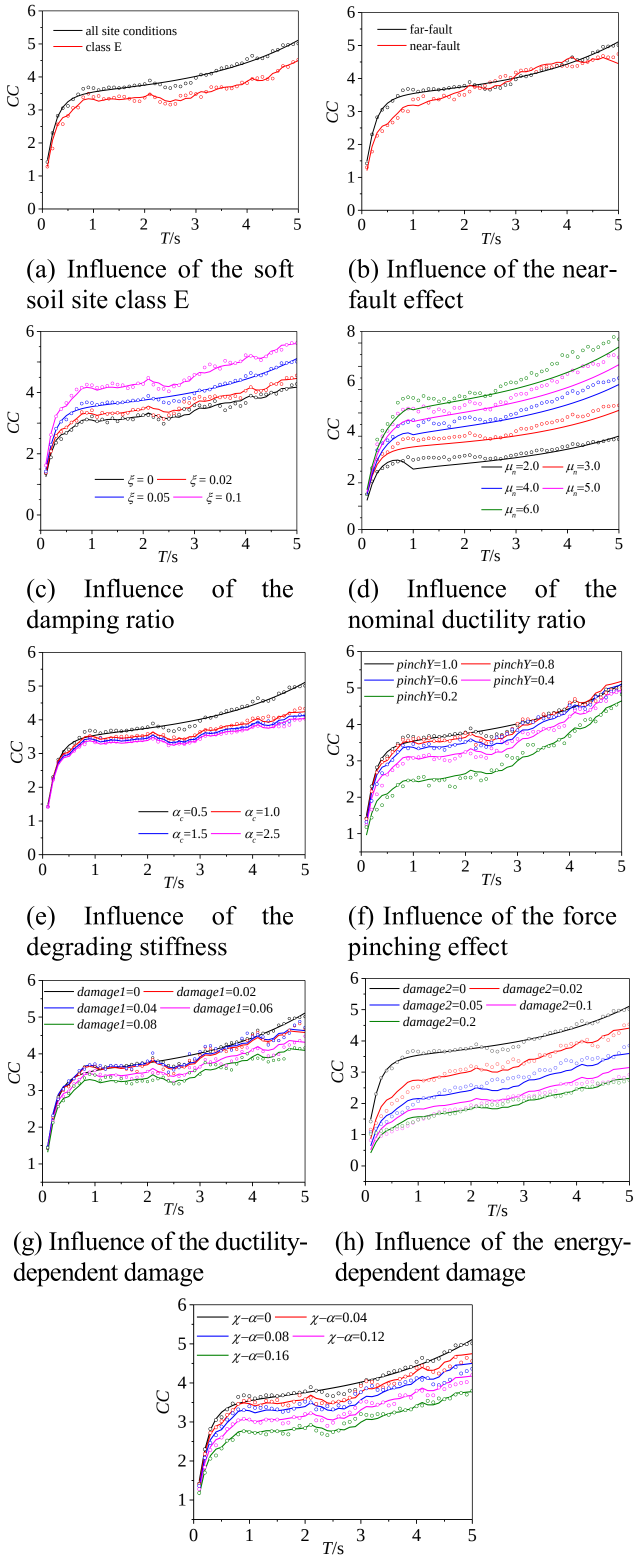

(a) Influence of the soft soil site class E

(b) Influence of the near-fault effect

(c) Influence of the damping ratio

(d) Influence of the nominal ductility ratio

(e) Influence of the degrading stiffness

(f) Influence of the force pinching effect

(g) Influence of the ductility-dependent damage

(h) Influence of the energy-dependent damage

(i) Influence of the P-delta effect

Fig. 14 Comparison between the fitting formulas and the statistical collapse capacity spectra

- Among the ground motion parameters, the soft site conditions (site E) impose relatively large influence on the seismic collapse capacity spectra, where the collapse capacity spectral values for site E are about 20% smaller than those from the other sites (site B, C, and D). The influences of earthquake magnitude and distance to rupture are proved to be negligible. Meanwhile, the near-fault effect may reduce the structural collapse capacity spectral values about 15% for structures with short periods.
- Among the structural parameters, the structural viscous damping ratio, nominal ductility ratio, degrading stiffness, strength pinching behavior, accumulated damage, and P-delta effect have considerable influences on the seismic collapse capacity spectra, especially the nominal ductility ratio and energy-dependent accumulated damage. While the influences of the displacement pinching behavior, and the unloading stiffness on the seismic collapse capacity spectra are negligible.
- The analytical formulas for the seismic collapse capacity spectra are presented considering both the influences of ground motion properties (soft site condition and near-fault effect), and structural properties (viscous damping ratio, nominal ductility ratio, degrading stiffness, strength pinching behavior, accumulated damage, and P-delta effect). Although the analytical formulas still need to be verified when multiple influences kick in simultaneously because they are evaluated separately for each considered factor, with the help of these fitted expressions, the structural collapse capacities could be easily predicted for future application in most situations.

Acknowledgements

This research project is supported by the National Natural Science Foundation of China (Grant No. 51578202, 51238012). The financial supports are greatly appreciated.

References

Adam, C. and Jäger, C. (2011), "Seismic induced global collapse of non-deteriorating frame structures", C*omputational Methods in Earthquake Engineering*, eds., Papadrakakis, M., Fragiadakis, M. and Lagaros, N.D., Springer, Dordrecht, 21-40.

Adam, C. and Jäger, C. (2012), "Seismic collapse capacity of basic inelastic structures vulnerable to the P-delta effect", *Earthq. Eng. Struct. Dyn.*, **41**(4), 775-793.

Alavi, B. and Krawinkler, H. (2004), "Behavior of moment-resisting frame structures subjected to near-fault ground motions", *Earthq. Eng. Struct. Dyn.*, **33**(6), 687-706.

Amara, F., Bosco, M., Marino, E.M. and Rossi, P.P. (2014), "An accurate strength amplification factor for the design of SDOF systems with P-Δ effects", *Earthq. Eng. Struct. Dyn.*, **43**(4), 589-611.

Ayoub, A. and Chenouda, M. (2009), "Response spectra of degrading structural systems", *Eng. Struct.*, **31**(7), 1393-1402.

Baker, J.W. (2007), "Quantitative classification of near-fault ground motions using wavelet analysis", *Bull. Seismol. Soc. Am.*, **97**(5), 1486-1501.

Borekci, M., Kirçil, M.S. and Ekiz, I. (2014), "Collapse period of degrading SDOF systems", *Earthq. Eng. Eng. Vib.*, **13**(4), 681-694.

Chopra, A.K. and Chintanapakdee, C. (2004), "Inelastic deformation ratios for design and evaluation of structures: Single-degree-of freedom bilinear systems", *J. Struct. Eng.*, ASCE, **130**(7), 1309-1319.

Dimakopoulou, V., Fragiadakis, M. and Spyrakos, C. (2013), "Influence of modeling parameters on the response of degrading systems to near-field ground motions", *Eng. Struct.*, **53**, 10-24.

Domizio M., Ambrosini D. and Curadelli O. (2015), "Experimental and numerical analysis to collapse of a framed structure subjected to seismic loading", *Eng. Struct.*, **82**, 22-32.

Esfahanian, A. and Aghakouchak, A.A. (2015), "On the improvement of inelastic displacement demands for near-fault ground motions considering various faulting mechanisms", *Earthq. Struct.*, **9**(3), 573-698.

FEMA (2000), "Recommended seismic design criteria for new steel moment-frame buildings", *Report # 350*, SAC Joint Venture, Federal Emergency Management Agency, Washington, DC.

Han, S.W., Ha, S.J., Moon, K.H. and Shin, M. (2014), "Improved capacity spectrum method with inelastic displacement ratio considering higher mode effects", *Earthq. Struct.*, **7**(4), 587-607.

Ibarra, L.F. and Krawinkler, H. (2011), "Variance of collapse capacity of SDOF systems under earthquake excitations", *Earthq. Eng. Struct. Dyn.*, **40**(12), 1299-1314.

Jäger, C. and Adam, C. (2013), "Influence of collapse definition and near-field effects on collapse capacity spectra", *J. Earthq. Eng.*, **17**(6), 859-878.

Katsanos, E.I. and Sextos, A.G. (2015), "Inelastic spectra to predict period elongation of structures under earthquake loading", *Earthq. Eng. Struct. Dyn.*, **44**(11), 1765-1782.

Lavan, O., Sivaselvan, M.V., Reinhorn A.M. and Dargush G.F. (2009), "Progressive collapse analysis through strength degradation and fracture in the Mixed Lagrangian Formulation", *Earthq. Eng. Struct. Dyn.*, **38**(13), 1483-1504.

Libel, A.B., Haselton, C.B. and Deierlein G.G. (2011), "Seismic collapse safety of reinforced concrete buildings. II: Comparative assessment of nonductile and ductile moment frames", *J. Struct. Eng.*, ASCE, **137**(4), 492-502.

Li, S. and Xie, L.L. (2007), "Effects of hanging wall and forward directivity in the 1999 Chi-Chi earthquake on inelastic displacement response of structures", *Earthq. Eng. Eng. Vib.*, **6**(1), 77-84.

Malhotra, P.K. (1999), "Response of buildings to near-field pulse-like ground motions", *Earthq. Eng. Struct. Dyn.*, **28**(11), 1309-1326.

Miranda, E. and Akkar, S.D. (2003), "Dynamic instability of simple structural systems", *J. Struct. Eng.*, ASCE, **129**(12), 1722-1726.

OpenSees (2015), *Open System for Earthquake Engineering Simulation*; Pacific Earthquake Engineering Research Center, University of California, Berkeley. http://opensees.berkeley.edu/wiki/index.php/Hysteretic_Material.

Rahgozar, N., Moghadam, A.S. and Aziminejad A. (2016), "Inelastic displacement ratios of fully self-centering controlled rocking systems subjected to near-source pulse-like ground motions", *Eng. Struct.*, **108**, 113-133.

Riddell, R., Garcia, J.E. and Garces, E. (2002), "Inelastic deformation response of SDOF systems subjected to earthquakes", *Earthq. Eng. Struct. Dyn.*, **31**(4), 515-538.

Shi, W., Lu, X.Z., Guan, H. and Ye, L.P. (2014), "Development of seismic collapse capacity spectra and parametric study", *Adv. Struct. Eng.*, **17**(9), 1241-1255.

Sivaselvan, M.V. (2013), "Hysteretic models with stiffness and strength degradation in a mathematical programming format", *Int. J. Non-Lin. Mech.*, **51**, 10-27.

Sivaselvan, M.V. and Reinhorn, A.M. (2000), "Hysteretic models for deteriorating inelastic structures", *J. Eng. Mech.*, ASCE, **126**(6), 633-640.

Thermou, G.E., Elnashai, A.S. and Pantazopoulou, S.J. (2012), "Retrofit Yield spectra - a practical device in seismic rehabilitation", *Earthq. Struct.*, **3**(2), 141-168.

Vamvatsikos, D. and Cornell C.A. (2002), "Incremental dynamic analysis", *Earthq. Eng. Struct. Dyn.*, **31**(3), 491-514.

Vian, D. and Bruneau, M. (2003), "Tests to structural collapse of single degree of freedom frames subjected to earthquake excitation", *J. Struct. Eng.*, ASCE, **129**(12), 1676-1685.

Villaverde, R. (2007), "Methods to assess the seismic collapse capacity of building structures: State of the art", *J. Struct. Eng.*, ASCE, **133**(1), 57-66.

Williamson, E.B. (2003), "Evaluation of damage and P-Δ effects for systems under earthquake excitation", *J. Struct. Eng.*, ASCE, **129**(8), 1036-1046.

Zareian, F. and Krawinkler, H. (2010), "Structural system parameter selection based on collapse potential of buildings in earthquakes", *J. Struct. Eng.*, ASCE, **136**(8), 933-943.

KT